Chapter 3

Study of Bi^{3+} assisted luminescence in $SrMoO_4:Sm^{3+}$ red phosphor

In this chapter we describe synthesis of pure $SrMoO_4$, Sm^{3+} (1% – 5%) doped $SrMoO_4$ and Bi^{3+} (1% – 3%) co-doped in 4% Sm^{3+} doped $SrMoO_4$ ($SrMoO_4:4Sm^{3+}$) phosphor by solution combustion method. The XRD analysis reveals the tetragonal phase of all samples, also Bi^{3+} co-doping supports crystallite size growth and reduces lattice strain. PL analysis ascertains an increase in emission peaks for Sm^{3+} doped $SrMoO_4$ up to 4% concentration. We have explained the effects of Bi^{3+} co-doping on the luminescence of Sm^{3+} doped $SrMoO_4$. The reduced microstrain and increased crystallinity of the phosphors as a result of Bi^{3+} co-doping and their correlation with the luminescence of Sm^{3+} ions are discussed.

i

3.1 Introduction

The inorganic phosphors doped with lanthanide (Ln^{3+}) ion have been studied by the research fraternity for their applications in display devices, white light-emitting diodes (wLEDs), plasma panel devices, etc. Apart from all the other applications, phosphor-based wLEDs are environment-friendly and energy-efficient. Commercially available wLED devices are made by fabricating InGaN as blue LED chip and coating YAG:Ce^{3+} yellow phosphor over it [53,91–93]. However, the lack of high color temperature and low color rendering index imposes limitations in their practical applications. This problem can be overcome either by using a combination of blue, green and red phosphor or using both red phosphor and yellow phosphor YAG:Ce^{3+} [55,57,58,94–96]. However, the large portion of emission from the above mentioned red phosphors lies beyond the human eye's long-wavelength limit (~700 nm), which imposes limitations on the use of these phosphors. Moreover, the synthesis process of these phosphors requires a high sintering temperature and reduced atmosphere which leads to several environmental issues and high investment imposing limitations on their large scale production. Therefore, the research to develop efficient, environmentally friendly, chemically, and thermally stable phosphor with a low-cost synthesis process is going on.

Among different phosphors, inorganic molybdates have gained the interest of researchers owing to their structural properties and their use as a luminescence material [97–101]. One such inorganic molybdate is $SrMoO_4$ which has a scheelite type crystalline structure and strong absorption in the ultraviolet (UV) region, thereby giving greenish-blue emission [22]. Apart from this particular advantage of $SrMoO_4$, other advantages include chemical stability, thermal stability, and low-cost synthesis [102]. In this study, we have synthesized $SrMoO_4$ (SMO) and doped $SrMoO_4$ by urea assisted solution combustion process as the synthesis route. The urea assisted solution combustion method is advantageous over other synthesis

processes owing to low heating temperature, cost-effectiveness, and environmental friendliness [103].

Over the past years, RE ion-doped phosphor materials have been studied because of the compelling optical properties owing to their 4f-4f transitions, the ligand to metal or metal to ligand charge transfer, and inter 5d-4f transitions [104,105]. The unique optical properties of RE ions have enabled their use in many emerging applications such as display panels, lighting appliances, biological applications, and lasers [16,106–108]. Among various red-emitting RE ions, Sm^{3+} has been explored as an activator in different host matrices [109–112]. The $^4G_{5/2} \rightarrow {}^6H_{J/2}$ (J=11, 9, 7, and 5) Sm^{3+} ion transitions gives reddish-orange emission [113,114]. The reddish-orange emission (560 nm to 645 nm) of Sm^{3+} ion lies within the wavelength sensitivity limit of the human eye, because of which the use of Sm^{3+} ion is advantageous over other red-emitting RE ions (Eu^{2+} and Ce^{3+}) is doped phosphors can be used as red-emitting phosphors [23]. Moreover, the near UV absorption of Sm^{3+} doped $SrMoO_4$ phosphor (around 404 nm) coincides with the blue-emitting GaN and InGaN chips used in wLED fabrication and therefore the Sm^{3+} doped $SrMoO_4$ phosphor can be is used with blue-emitting chips for the realization of white light [23]. Recently, Bi^{3+} ion has been studied as an excellent sensitizer for lanthanide ions with f-f transitions [115]. The Bi^{3+} ion absorbs UV light owing to its transition from $^1S_0 \rightarrow {}^3P_1$. It can then transfer energy to lanthanide activators, which improves their luminescence intensity significantly. The efficient enhancement of different emission peaks of Sm^{3+} ions by the non-sensitization effect of Bi^{3+} ions is also reported [116]. However, the structural analysis of SMO:Sm^{3+}, Bi^{3+} and energy transfer (ET) mechanism in Bi^{3+} and Sm^{3+} ions in $SrMoO_4$ phosphor, leading to photoluminescence enhancement, have not been investigated and is thus studied by us.

In the present work, we have synthesized series of SMO:Sm^{3+}, Bi^{3+} phosphors by the facile urea assisted solution combustion process. All the prepared phosphors were characterized by structural and optical characterization techniques. The PL spectra of all samples reveal the enhancement in the luminescence intensity for a particular concentration of Bi^{3+} ions in SMO:Sm^{3+}. The energy transfer mechanism and a possible connection between the results of PL and structural study are investigated.

3.2 Materials and synthesis technique

3.2.1 Materials and preparation of Bi^{3+}, Sm^{3+} co-doped $SrMoO_4$ phosphors.

The Bi^{3+}, Sm^{3+} doped and co-doped $SrMoO_4$ phosphors have been synthesized via the solution combustion process. Strontium oxide (SrO, 99.9%, Sigma-Aldrich), ammonium molybdate (para) tetrahydrate ($(NH_4)_6Mo_7O_{24}.4H_2O$, 99.98%, Sigma-Aldrich), samarium nitrate ($Sm(NO_3)_3$, 99.999%, Sigma-Aldrich), bismuth nitrate ($Bi(NO_3)_3$, 98%, Sigma-Aldrich) were taken as starting materials. The combustion was facilitated by using urea. We have synthesized pure strontium molybdate, Sm^{3+} (1%, 3%, 4%, 5%) doped $SrMoO_4$ and Sm^{+3} (4%) doped $SrMoO_4$ co-doped with Bi^{3+} concentrations (1%, 2%, and 3%) having code names SMO, SMS1, SMS3, SMS4, SMS5, SMB1, SMB2 and SMB3, respectively. The procedure for sample preparation is discussed in chapter 2.

3.2.2 Characterizations

All the prepared phosphors were initially characterized by XRD using the Rigaku-MiniFlex-II DESKTOP powder X-ray diffractometer equipped with Cu K_α radiation (λ=1.54Å). The XRD patterns have been recorded over the range of $20^0 \leq 2\theta \leq 120^0$ with an interval of 0.02º. The Energy dispersive X-ray (EDX) spectra have been obtained by using a High-Resolution Scanning electron microscope, EDAX Inc. The Fourier transform infrared (FTIR) spectra have been recorded by using JASCO FT/IR 4600. UV-Vis

absorption spectra of all the phosphors were recorded over the range of 200 nm – 800 nm by using JASCO V770 UV-Vis-NIR spectrophotometer. Photoluminescence (PL) spectra and lifetime have been recorded using the Horiba Fluorolog-3 spectrophotometer equipped with 450w xenon flash lamp.

3.3. Results and discussion

3.3.1 X-ray diffraction analysis

Fig. 3.1 presents the Rietveld refined XRD patterns of SMO, SMS4, and SMB2 calcined at 1000 ℃ in air. The XRD patterns confirm the tetragonal phase of the prepared phosphors. Some of the prominent diffraction peaks such as (112), (004), (200), (211), (204), (220), (116), (312) and (136) are indexed as tetragonal crystal structure having $I4_1/a$ space group (JCPDS file No. 85-0586 (a=b=5.394 Å and c=12.020 Å)) [117]. The refinement pattern shows a small impurity peak corresponding to $SrCO_3$ [marked as * in Fig. 3.1]. The ionic radius of Sm^{3+} (1.079 Å) and Bi^{3+} (1.17 Å) for the system of coordination number = 8 is closer to that of Sr^{2+} (1.26 Å) than that of Mo^{6+} (0.41 Å) [118], therefore, it is expected that Sm^{3+} and Bi^{3+} ions are substituted in Sr^{2+} site. In $SrMoO_4$, Mo atoms are co-ordinated with four oxygen atoms to form $[MoO_4]^{2-}$ tetrahedrons and Sr atoms are co-ordinated with eight oxygen atoms to form $[SrO_8]$ clusters. The lattice parameters and volume of all the prepared phosphors are obtained using FULLPROF software [119] and are listed in Table 3.1 and 3.2. Since the ionic radius of Sm^{3+} is lower than that of Sr^{2+}, it is observed that the XRD peaks shift towards a higher angle with Sm^{3+} doping up to SMS4, which indicates that Sm^{3+} ions have been substituted in Sr^{2+} sites. After Rietveld refinement, we have observed that the lattice parameters are decreased by Sm^{3+} doping, which is consistent with earlier reports [120]. The decrease in lattice parameters is because the ionic radius of Sm^{3+} (1.079 Å) is lower than ionic radius of Sr^{2+} (1.26 Å) ions, which again ascertains that Sm^{3+} ions have occupied the sites of Sr^{2+} ions [120]. The decrease in lattice parameters is also observed after Bi^{3+} ion

co-doping. The decrease in the lattice parameters of the unit cell after doping results in the contraction of unit cell volume.

Table 3.1 Structural parameters obtained after Rietveld refinement of Sm^{3+} doped $SrMoO_4$.

Parameters	**SMO**	**SMS1**	**SMS3**	**SMS4**	**SMS5**
Atomic positions (x,y,z)*:*					
Sr/Sm/Bi	(0,1/4,5/8)	(0,1/4,5/8)	(0,1/4,5/8)	(0,1/4,5/8)	(0,1/4,5/8)
Mo	(0,1/4,1/8)	(0,1/4,1/8)	(0,1/4,1/8)	(0,1/4,1/8)	(0,1/4,1/8)
O	(0.2414,0.1178,0.0468)	(0.2375,0.1100,0.0488)	(0.2395,0.1100,0.0476)	(0.2383,0.1092,0.0476)	(0.2372,0.1078,0.0484)
Angles (α, β, γ) in degree	(90, 90, 90)	(90, 90, 90)	(90, 90, 90)	(90, 90, 90)	(90, 90, 90)
Lattice parameters (Å)					
a	5.397	5.396	5.397	5.395	5.396
c	12.026	12.023	12.025	12.015	12.021
Unit cell volume ($Å^3$)	350.34	350.07	350.25	349.75	350.01
Bond lengths (Å)					
Sr/Sm/Bi-O1	2.593(3)	2.572(4)	2.573(4)	2.571(3)	2.567(4)
Sr/Sm/Bi-O2	2.602(3)	2.636(3)	2.618(3)	2.622(3)	2.635(4)
Mo-O	1.759(3)	1.746(4)	1.763(4)	1.759(3)	1.753(4)
$R_{Factors}$					
R_p	7.47	8.24	8.61	7.95	8.97
R_{wp}	8.05	8.58	8.91	8.35	9.57
χ^2	4.83	5.82	5.70	5.00	6.38

Table 3.2 Structural parameters obtained after Rietveld refinement of Bi^{3+} doped $SrMoO_4$:4 Sm^{3+}.

Parameters	**SMB1**	**SMB2**	**SMB3**
Atomic positions (x,y,z):			
Sr/Sm/Bi	(0,1/4,5/8)	(0,1/4,5/8)	(0,1/4,5/8)
Mo	(0,1/4,1/8)	(0,1/4,1/8)	(0,1/4,1/8)
O	(0.239,0.111,0.044)	(0.239,0.112,0.044)	(0.235,0.110,0.044)
Angles (α, β, γ) in degree	(90, 90, 90)	(90, 90, 90)	(90, 90, 90)
Lattice parameters (Å)			
a	5.395	5.395	5.394
c	12.020	12.018	12.015
Unit cell volume $(Å^3)$	349.94	349.83	349.62
Bond lengths (Å)			
Sr/Sm/Bi-O1	2.590(4)	2.596(3)	2.597(4)
Sr/Sm/Bi-O2	2.586(4)	2.586(3)	2.602(4)
Mo-O	1.780(4)	1.774(3)	1.762(4)
$R_{Factors}$			
R_p	8.04	9.31	8.56
R_{wp}	8.54	9.95	9.49
χ^2	4.79	6.24	6.02

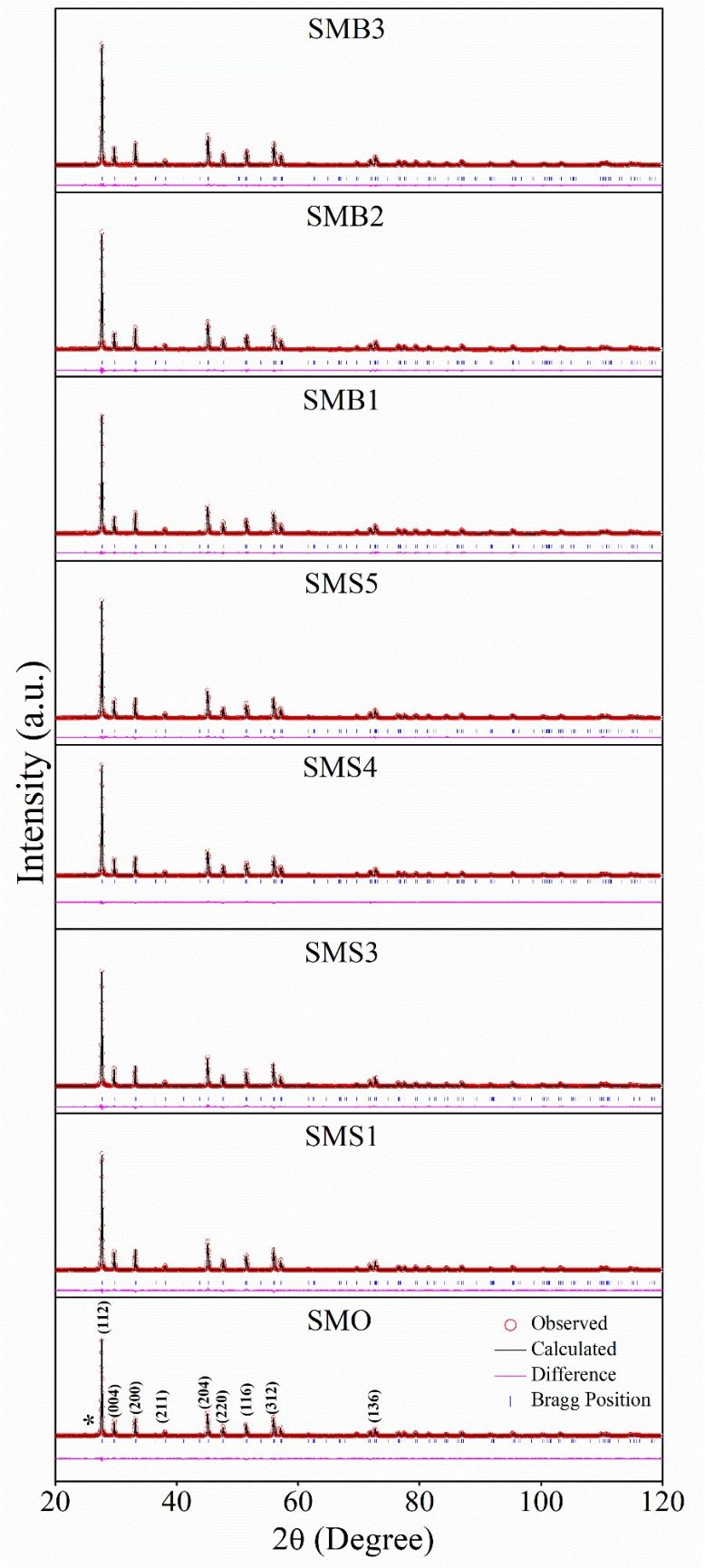

Fig. 3.1 Rietveld refined XRD plots of SMO, SMS4 and SMB2.

The XRD pattern can be used to estimate the crystallite size of the sample. We have employed the Williamson-Hall (W-H) method to estimate the crystallite size (D), which takes lattice strain (ϵ) into account. The well-known Williamson-Hall expression is given by equation 3.1,

$$\beta cos\theta = 4\epsilon sin\theta + \frac{K\lambda}{D}, \tag{3.1}$$

Where β is calculated Full width at half maximum (FWHM) obtained by deducting instrumental broadening ($\beta_{\text{instrumental}}$) from the FWHM ($\beta_{\text{measured}}$) of XRD peak pattern, θ is the corresponding angle of the examined peak, λ is the wavelength ($\lambda = 0.154$ nm) of X-ray, and K is the shape factor (K~ 0.9) [121]. The W-H expression represents a linear equation, where the intercept is used to obtain the crystallite size (D) and the slope calculated from the linearly fitted line gives the microstrain (ε). The variation of crystallite size and strain with samples is presented in Fig. 3.2 and tabulated in Table 3.3. The crystallite size of $SrMoO_4$ is found to be 57 nm which reduces by doping Sm^{3+} ions. Further, an increase in crystallite size is observed in Bi^{3+} co-doped $SrMoO_4:4Sm^{3+}$. The increase in crystallite size suggests that the crystallinity of the phosphors is increased after Bi^{3+} co-doping and thereby reduces the density of grain boundaries. The grain boundaries are the source of light adsorption generated inside, therefore, reducing grain boundaries is favourable for luminescence enhancement [121].

The microstrain (ε), which is a measure of crystal lattice relaxation is also estimated from the W-H plot. The calculated value of ε for $SrMoO_4$ is found to be 0.0034 and increases with increasing Sm^{3+}doping but further decreases with Bi^{3+} co-doping. The decrease in microstrain is an indication of decrease in the crystal defects present in the phosphor which suggest improvement in the local crystal structure of the phosphor with Bi^{3+} co-doping. The ordering of crystal structure help in improving the emission intensity [122].

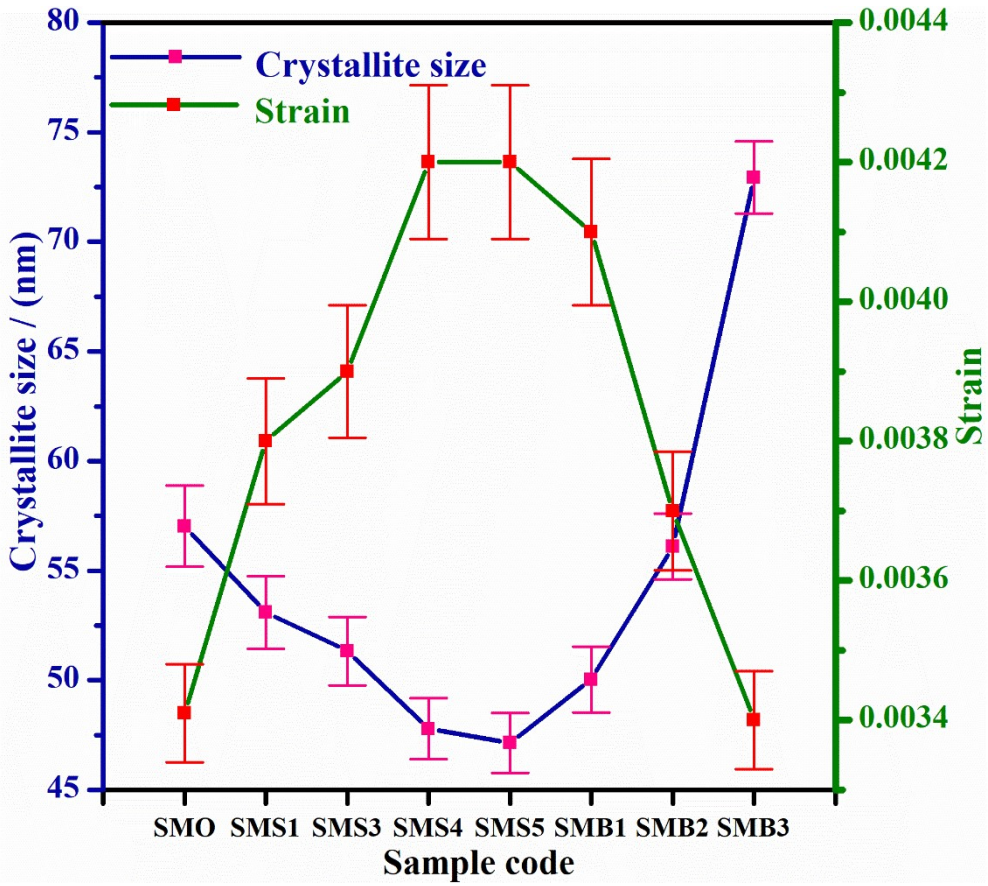

Fig. 3.2 The crystallite size and strain variation with samples obtained after their W-H plot analysis.

Table 3.3 Crystallite size (D) and strain (ε) values for all samples.

Sample code	Crystallite size (nm)	Strain (%)
SMO	57	0.34
SMS1	53	0.38
SMS3	51	0.39
SMS4	48	0.42
SMS5	47	0.42
SMB1	50	0.41
SMB2	56	0.37
SMB3	73	0.34

3.3.2 Energy dispersive X-ray analysis

The EDX spectra have been used to obtain the presence of elements in SMB2 phosphor. The spectra depicted in Fig. 3.3 is used to manifest the existence of Sr, Mo, O, Sm, and Bi elements in the phosphor. We have not detected any elemental impurity in the sample. The weight percentage of elements present in EDX spectra of SMB2 are tabled in the inset of Fig. 3.3.

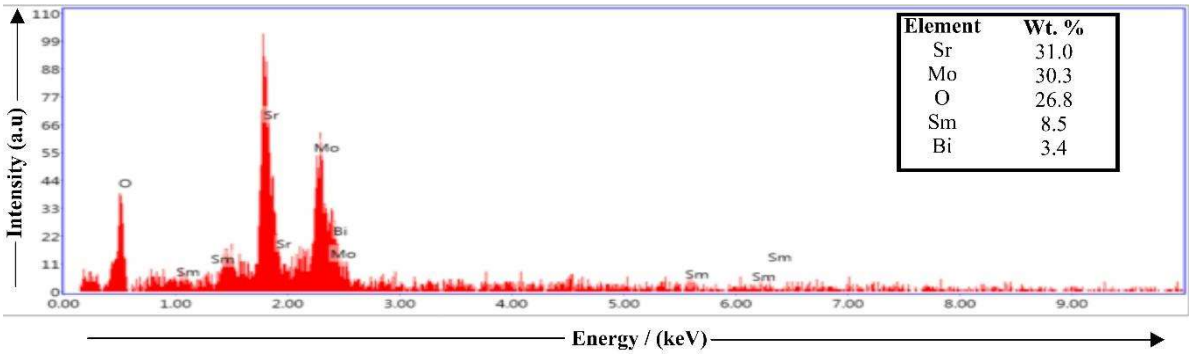

Fig. 3.3 Energy dispersive X-ray spectra SMB2 phosphor.

3.3.3 FT-IR study

The vibrational modes of the synthesized phosphors were studied by recording their FTIR spectra at room temperature. The scheelite-type $SrMoO_4$ have 26 different vibrational modes represented as:

$$\Gamma = A_1(\nu_1) + E(\nu_2) + F_2(\nu_3) + F_2(\nu_4). \quad (3.2)$$

The $A_1(\nu_1)$ and $E(\nu_2)$ vibrational modes are Raman active whereas, $F_2(\nu_3, \nu_4)$ modes are Infrared active [123]. The recorded FTIR spectra for SMO, SMS4, and SMB2 samples within the wavenumber range 360 cm^{-1} to 4000 cm^{-1} is depicted in Fig. 3.4.

The intense broadband from 430 cm^{-1} to 900 cm^{-1} corresponds to the $F_2(\nu_3)$ antisymmetric stretched vibrations of Mo—O bond in the MoO_4^{2-} tetrahedral clusters. The band around 400 cm^{-1} corresponds to less intense $F_2(\nu_4)$ bending vibrational mode of O—Mo—O bonds

in MoO_4^{2-} tetrahedral clusters [123,124]. It is observed that the two bonds involving Mo and O are not shifted with doping. The vibrational band from 2340 cm^{-1} to 2360 cm^{-1} is due to the adsorbed atmospheric carbon dioxide [125]. The vibrational band around 1652 cm^{-1} is attributed to O—H—O bending vibrations of H_2O present on the surface of the microcrystals [126]. The band around 1506 cm^{-1} is attributed to NO_3^- stretching vibrations [127]. The observed vibrational bands of the molybdate ion $[MoO_4]^{2-}$ suggest that the crystalline phase of SMO and doped SMO has formed and thus confirms the XRD results.

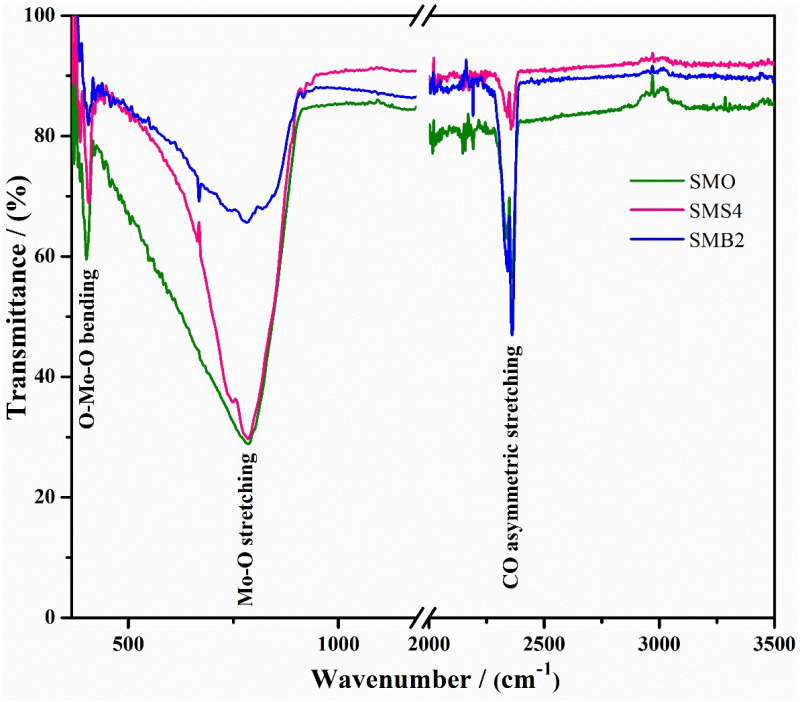

Fig. 3.4 FTIR spectra of SMO, SMS4 and SMB2.

3.3.4 Absorption study

The UV-Vis absorption spectra of all the phosphors recorded over the wavelength range of 200 nm to 800 nm is depicted in Fig. 3.5 (a). The absorption band for SMO centered on 260 nm is observed, which is the charge transfer band (CTB) accredited to charge transfer from O^{2-} to Mo^{6+} [128]. The Sm^{3+} doped samples show a small shift in the absorption peak towards the higher wavelength, which results in a decrease in the bandgap. Again the intense absorption band for Sm^{3+} doped samples is the result of the overlap of the CTBs

accredited to charge transfer from O^{2-} to Mo^{6+} and O^{2-} to Sm^{3+}. For Sm^{3+} doped samples, a peak is observed around 404 nm owing to $^6H_{5/2} \rightarrow {}^4F_{7/2}$ transition of Sm^{3+} ions [113]. For Bi^{3+} co-doped samples, we have observed a peak around 308 nm which increases with increasing concentration of Bi^{3+}. The peak around 308 nm is ascribed to Bi^{3+} transitions. A similar observation of peak redshift by Bi^{3+} doping has been observed by Wang et al. [129].

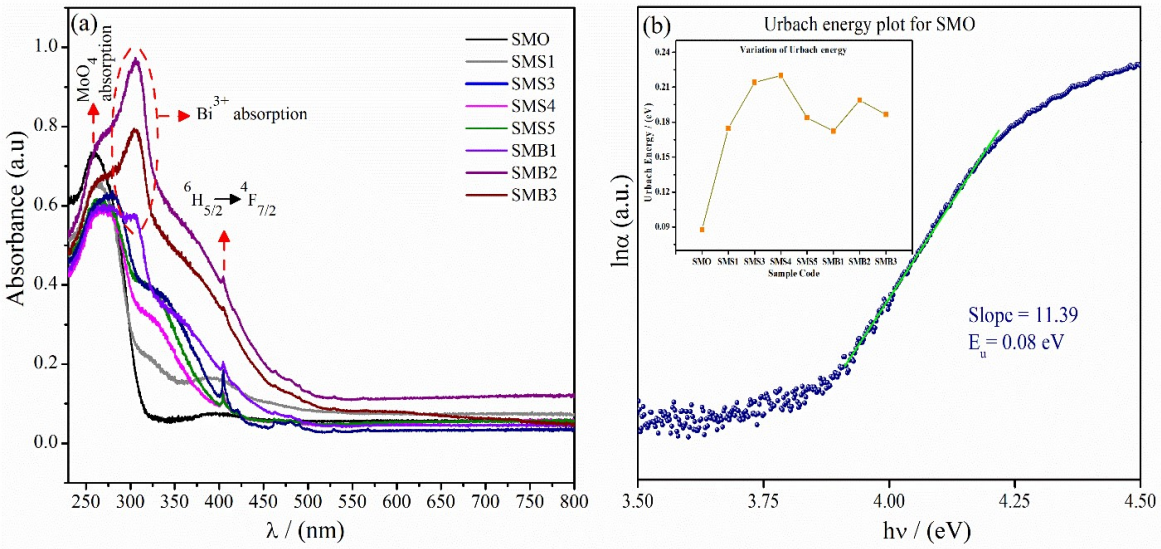

Fig. 3.5 (a) Absorption spectra of all the prepared phosphors. **(b)** Urbach tail width plot for SMO. Inset shows variation of Urbach energy with samples.

The optical band gap (E_g) for all the samples have been calculated by using Wood and Tauc formula given in equation 3.3 [125,130,131],

$$\alpha h\vartheta = A(h\vartheta - E_g)^n, \tag{3.3}$$

Where α and $h\vartheta$ are the absorption coefficient and the incident photon energy, respectively. The electronic transitions for $SrMoO_4$ are of direct allowed type, therefore the value of n is taken to be ½ [132]. The $(\alpha h\vartheta)^2$ versus $(h\vartheta)$ plot is used to ascertain the bandgap of all the samples and is shown in Fig. 3.6.

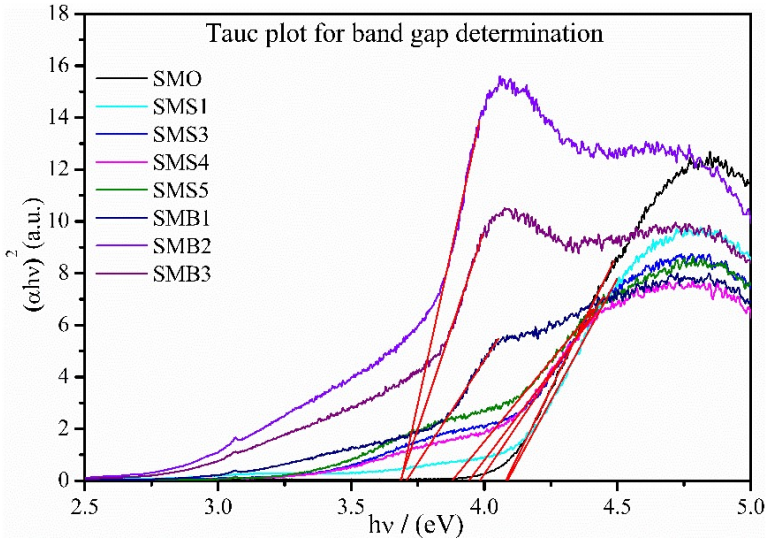

Fig. 3.6 Tauc plot for all samples.

The x-intercept for $(\alpha h\vartheta)^2=0$ gives the optical band gap. The optical band gap of SMO is approximated as 4.0 eV, which is similar to as reported by Li et al. [132]. For the Sm^{3+} doped samples, we have noticed that the bandgap is slightly reduced up to 3.8 eV for SMS5. The results from XRD analysis suggest that by increasing the percentage of Sm^{3+}doping in $SrMoO_4$, the crystallinity is deteriorated. As a result of which, site defects are generated in the microcrystals creating intermediate defect energy levels which reduces the bandgap. A similar variation in bandgap with crystallinity is reported by Park et al. [125]. The co-doping of Bi^{3+} ions in SMS4 further reduces the bandgap to 3.7 eV. The reduction in the optical bandgap of the host by Bi^{3+} doping has been reported by Yadav et al. The Bi^{3+} ions create defect energy levels below the conduction band of the host, which facilitates the flow of charges from O^{2-} orbital to Bi^{3+} orbitals [133]. Thus, we can say that energy levels Bi^{3+} ions match well with that of MoO_4^{2-}, inducing effective energy transfer from MoO_4^{2-} to excited energy levels of Bi^{3+} ions.

The doping of Sm^{3+} and Bi^{3+} ions in $SrMoO_4$ crystal lattice create defect centers in the lattice due to mismatch of ionic radius between the Sm^{3+}/Bi^{3+} and Sr^{2+} ions. These defects create localized states between the bandgap. The Urbach energy (E_u) can substantiate the

creation of defect states within the bandgap. The fundamental absorption edge obey the exponential Urbach rule and E_u is given by the following equation 3.4 [131],

$$\alpha = \alpha_0 e^{\left(\frac{h\vartheta}{E_u}\right)} \tag{3.4}$$

Where, α denotes absorption coefficient, α_0 is a constant and $h\vartheta$ represents the incident photon energy. The Urbach energy is deduced from the reciprocal of the slope of the linear part of $\ln(\alpha)$ vs $h\vartheta$ plot. Fig. 3.5 (b) depicts the $\ln(\alpha)$ vs $h\vartheta$ plot for SMO and the inset in Fig. 3.5 (b) shows the variation of Urbach energy with samples. It is observed that the Urbach energy for SMO is 0.08 eV and increases with doping Sm and Bi ions in the host, which is a clear validation of the creation of localized states within the bandgap of the host [131]. The value of E_g and E_u for all samples are listed in Table 3.4.

Table 3.4 Calculated optical bandgap (E_g) and Urbach energy (E_u) for all samples.

Sample code	**Optical bandgap (eV)**	**Urbach energy (eV)**
SMO	4.0	0.08
SMS1	4.0	0.17
SMS3	3.9	0.21
SMS4	3.9	0.22
SMS5	3.8	0.18
SMB1	3.7	0.17
SMB2	3.7	0.20
SMB3	3.7	0.18

3.3.5 Photoluminescence study

The photoluminescence excitation (PLE) spectra for $SrMoO_4$ recorded at 495 nm emission wavelength is depicted in Fig. 3.7.

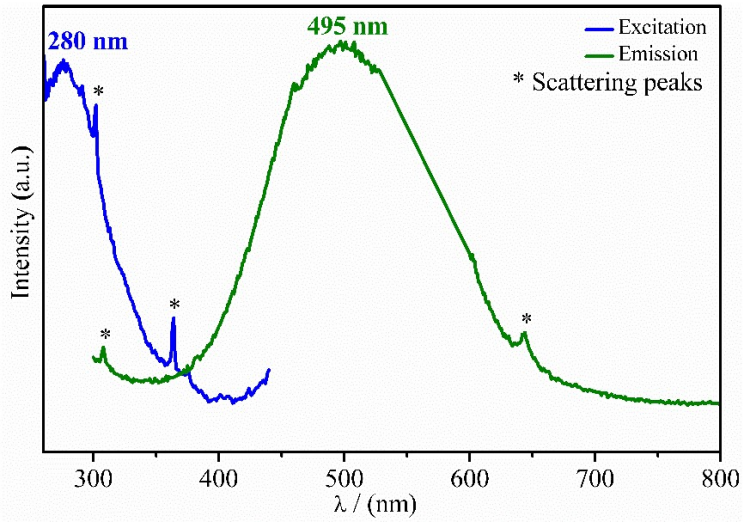

Fig. 3.7 Photoluminescence excitation and emission spectra for $SrMoO_4$.

The broadband observed at around 280 nm for $SrMoO_4$ is accredited to charge transfer from O^{2-} to Mo^{6+} in MoO_4^{2-} groups, which is termed as a ligand to metal charge transfer (LMCT) band. The PLE spectra for Sm^{3+} doped $SrMoO_4$ are presented in Fig. 3.8 (a). The PLE spectra for SMS series were recorded by monitoring $^4G_{5/2} \rightarrow {}^6H_{9/2}$ emission transition of Sm^{3+} ion.

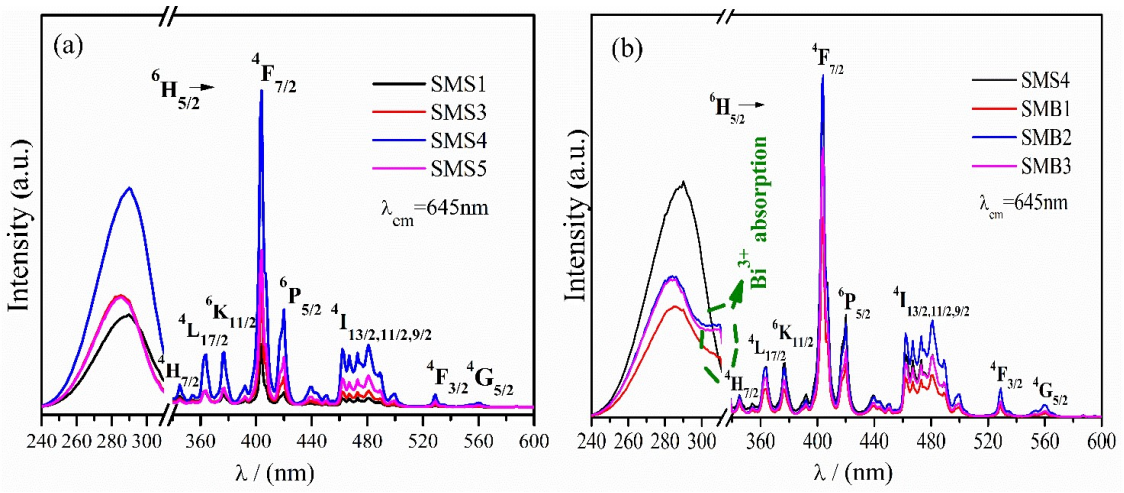

Fig. 3.8 (a) PLE spectra for Sm^{3+} doped $SrMoO_4$ phosphors for 645 nm emission wavelength. **(b)** PLE spectra for Bi^{3+} co-doped phosphors for 645 nm emission wavelength.

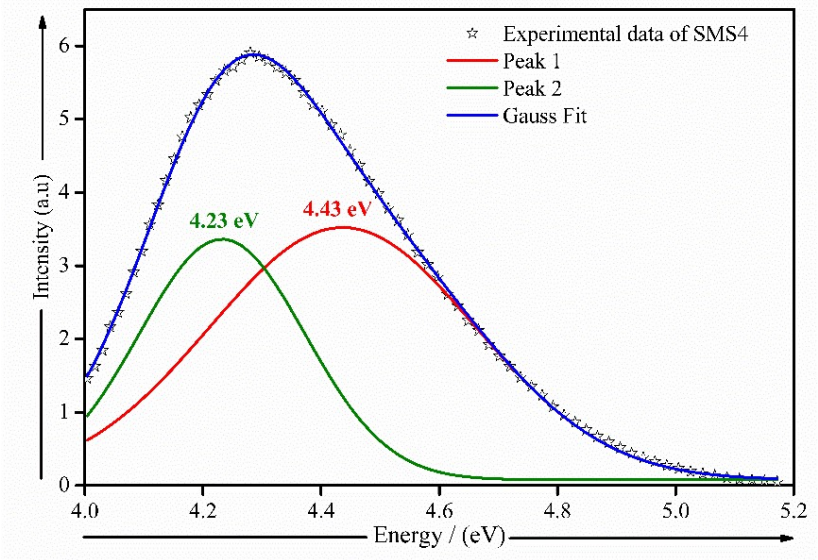

Fig. 3.9 Deconvoluted broadband PLE spectra of SMS4 in 250 – 310 nm wavelength range.

Fig. 3.9 depicts the PLE broadband of SMS4, centered at 290 nm (4.28 eV), which shows that PLE broadband can be deconvoluted into two peaks at 280 nm (4.43 eV) and 293 nm (4.23 eV), respectively. The first peak around 280 nm corresponds to LMCT band of O^{2-} to Mo^{6+} in MoO_4^{2-} groups and the second peak around 293 nm corresponds to CTB of O^{2-} to Sm^{3+} ions. Therefore, the overlap of LMCT band and CTB results in the broadband from 260 to 310 nm. The CTB is accredited to the electron transfer from filled 2p orbital of O^{2-} to the partially filled orbital of the Sm^{3+} ions. We have observed some characteristic intra f-f transitions of Sm^{3+} ions centered at 345 nm, 364 nm, 377 nm, 404 nm, 420 nm, 462-481 nm, 529 nm, and 561 nm, corresponding to transitions from the $^6H_{5/2} \rightarrow {}^4H_{7/2}$, $^6H_{5/2} \rightarrow {}^4L_{17/2}$, $^6H_{5/2} \rightarrow {}^6K_{11/2}$, $^6H_{5/2} \rightarrow {}^4F_{7/2}$, $^6H_{5/2} \rightarrow {}^6P_{5/2}$, $^4I_{13/2,11/2,9/2}$, $^6H_{5/2} \rightarrow {}^4F_{3/2}$, and $^6H_{5/2} \rightarrow {}^4G_{5/2}$, respectively. The strongest excitation band obtained from the PLE spectrum is around 404 nm, which makes Sm^{3+} doped $SrMoO_4$ phosphors the potential candidate for wLEDs because it covers the emission band of commercial blue LED chips. Similar observations for $O^{2-} \rightarrow Mo^{6+}$ LMCT band, O^{2-} to Sm^{3+} ions CTB and other Sm^{3+} ion transitions have been reported by other research groups [17,47,113,129]. The PLE spectra for Bi^{3+} co-doped samples compared with SMS4 are depicted in Fig. 3.8 (b). The excitation band intensity around 404

nm is maximum for SMB2, while the intensity of broadband for the same is less than that of SMS4. On addition of Bi^{3+} to SMS4, Bi^{3+} and Mo^{6+} ions form Bi^{3+}–Mo^{6+} metal-metal charge transfer (MMCT) band and its overlap with O^{2-} to Sm^{3+} CTB results in broadband centered on 290 nm [134]. The PLE spectra for all Bi^{3+} co-doped samples have broadening around 308 nm which is attributed to the $^1S_0 \rightarrow {}^3P_1$ transition of Bi^{3+} [135].

The photoluminescence emission (PL) spectra for $SrMoO_4$ is depicted in Fig. 3.7. The PL spectra for $SrMoO_4$ was recorded at 280 nm excitation wavelength. The broadband observed from 450 nm to 550 nm is accredited to the charge transfer within $[MoO_4]^{2-}$. The PL spectra for Sm^{3+} doped $SrMoO_4$ are presented in Fig. 3.10 (a). The PL spectra for SMS series have been recorded for 404 nm excitation wavelength in the range of 500 – 750 nm. The PL spectra show emission peaks centered at 562 nm, 600 nm, 645 nm, and 705 nm, corresponding to the transitions from $^4G_{5/2} \rightarrow {}^6H_{5/2}$, $^4G_{5/2} \rightarrow {}^6H_{7/2}$, $^4G_{5/2} \rightarrow {}^6H_{9/2}$, and $^4G_{5/2} \rightarrow {}^6H_{11/2}$, respectively. The phosphors give reddish-orange emission with the strongest emission peak centered at 645 nm.

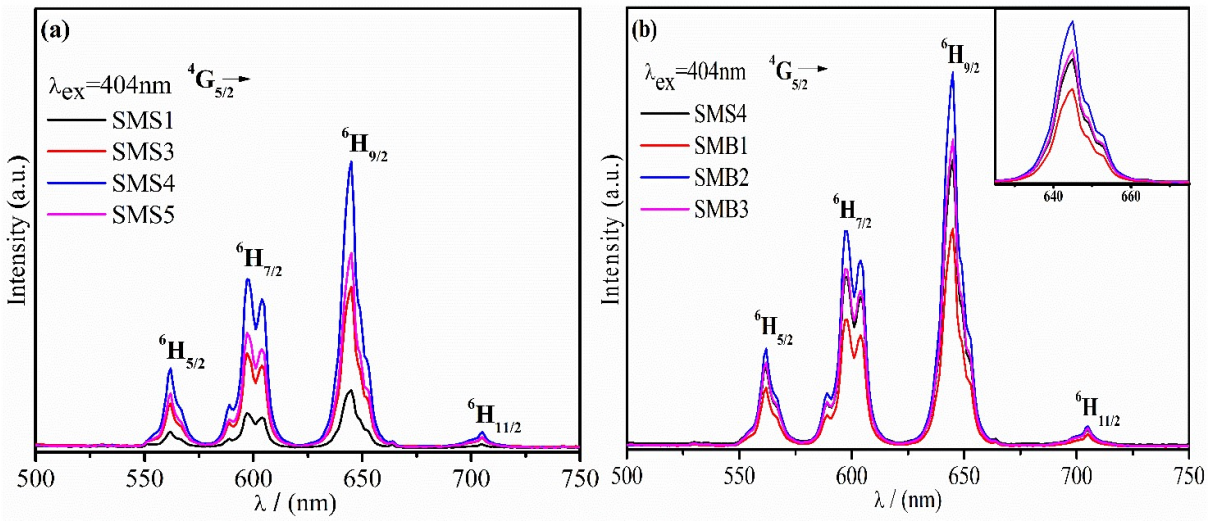

Fig. 3.10 (a) PL spectra for Sm^{3+} doped $SrMoO_4$ upon 404 nm excitation wavelength. **(b)** Comparative PL spectra of Bi^{3+} co-doped $SrMoO_4:4Sm^{3+}$ and $SrMoO_4:4Sm^{3+}$ phosphors upon 404 nm excitation wavelength.

A similar observation of Sm^{3+} emission peaks is reported by Xiong et al. for Sm^{3+} doped $LnBWO_6$ phosphor [109]. The emission peak splitting at 600 nm is because of the crystal field and a similar observation is reported by Wu et al. [113]. The peak corresponding to $^4G_{5/2} \rightarrow {}^6H_{9/2}$ transition at 645 nm is attributed to electric dipole transition and is influenced by the local symmetry of Sm^{3+} ions. The dominance of the 645 nm peak over other emission peaks indicates that the electric dipole transition is dominant and Sm^{3+} ions occupy a lower symmetry site in the host lattice [135]. It is observed that the emission peak intensity increases with Sm^{3+} concentration and is maximum for SMS4 and decreases afterward owing to concentration quenching. We conclude that the optimum Sm^{3+} concentration is 4 %, after which intensity decreases because of concentration quenching. Usually, the quenching process among the luminescent centers is possible via two mechanisms, (i) the exchange interaction, and (ii) electric multipolar interaction. The exchange interaction is possible when the wave-functions of the donor and the acceptor overlap after a critical distance (R_c) and the energy transfer among the ions increases. The R_c between Sm^{3+} ions in $SrMoO_4$ at which energy transfer occurs is estimated using the relation in equation 3.5 [136,137],

$$R_c = 2\left(\frac{3V}{4\pi x_c N}\right)^{\frac{1}{3}} \tag{3.5}$$

Where, V denotes the volume of the unit cell and is estimated to be 350.34 $Å^3$ from XRD analysis, critical concentration (x_c) is the concentration of Sm^{3+} after which the quenching starts, and N denotes the number of available lattice sites for the dopant to be occupied in a unit cell. The critical concentration of $SrMoO_4$:$4Sm^{3+}$ is 0.04 and N for $SrMoO_4$ is 4. The calculated critical distance (R_c) is 16.11 Å. Since, exchange interaction require large overlap of the wavefunctions of the donor and acceptor ions, the critical distance must be in range of 5 Å [136,137]. Thus, the calculated value of R_c suggest that the non-radiative ET is not the result of exchange interaction but can be because of electric multipolar interactions.

Fig. 3.10 (b) depicts a comparison of PL spectra between Bi^{3+} co-doped SMS4 and SMS4, recorded for 404 nm excitation wavelength in the range 500 – 750 nm. We have observed that the intensity of the SMB2 phosphor is maximum. The overall increase in emission peak intensity corresponding to 645 nm wavelength is 30% relative to SMS4. The increase in the intensity of emission peak of SMB2 when excited with 404 nm is accredited to the non-sensitization effect of Bi^{3+} ions. From the XRD analysis we infer that with increasing Bi^{3+} concentration, the crystallinity of the phosphor is improved. The increased crystallinity, increased particle size and reduced microstrain contribute towards increasing the PL emission. The defect centers act as quenching centers for excited ions, as some of their energy is transferred to these defects and relax non-radiatively to the ground state. Therefore, nonradiative relaxation increases with increase in defect centers. It is observed that the particle size increases with increase in crystallinity, which consequently decreases the surface to volume ratio [138]. As the defect centers are larger at the surface of particles, hence with decrease in the total surface area, the number of ions interacting with defect centers also decrease. Therefore, increase in crystallinity will increase the number of emitting ions in the crystallites, while decreasing the total surface area and defect centers. These factors helps in increasing the emission intensity [121,138,139]. Secondly, Bi^{3+} co-doping decreases the microstrain which decreases the crystal defects present in the phosphor because of which crystal structure becomes more ordered. The ordering of crystal structure improves the emission intensity [122]. Therefore, by improving the crystallinity and reducing microstrain, Bi^{3+} ions increase the luminescence intensity of Sm^{3+} ions.

The Bi^{3+} co-doped SMS4 phosphors were also excited by 308 nm excitation wavelength for examining the role of Bi^{3+} ions as sensitizer. The PL spectra Bi^{3+} co-doped SMS4 phosphors and SMS4 in the range 500 —750 nm is shown in Fig. 3.11 (a).

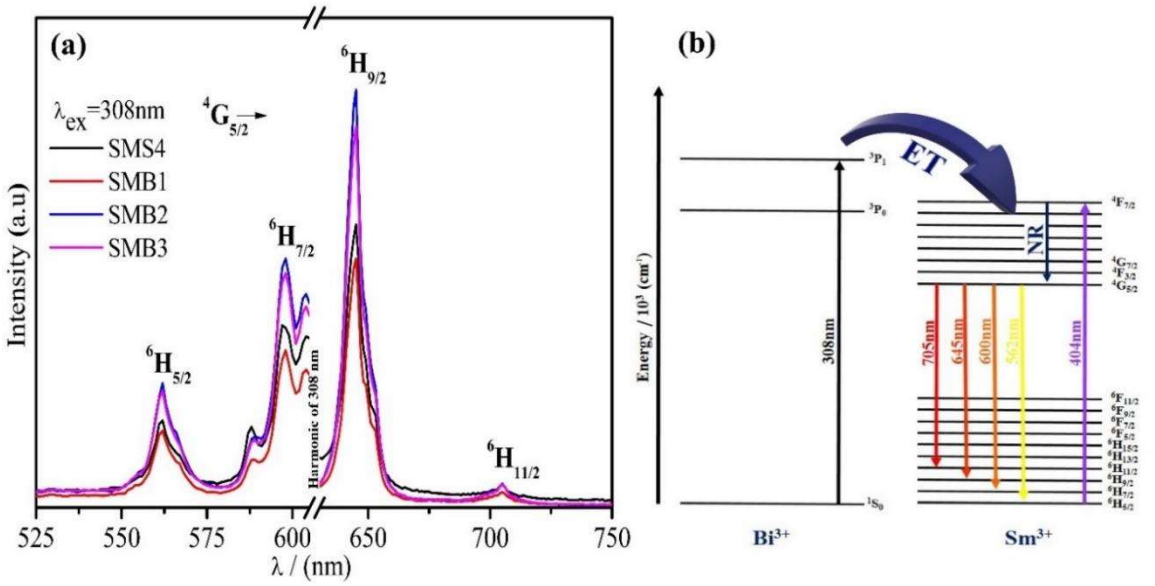

Fig. 3.11 (a) Comparative PL spectra of Bi^{3+} co-doped $SrMoO_4:4Sm^{3+}$ and $SrMoO_4:4Sm^{3+}$ phosphors upon 308 nm excitation wavelength. **(b)** The energy level diagram showing energy transfer mechanism from Bi^{3+} to Sm^{3+} ions.

All the peak positions are similar, however, the PL emission is increased upto 1.5 times compared to that of phosphors with 404 nm excitation. This increase can be due to ET from $^3P_1$ level of Bi^{3+} ions to energy levels of Sm^{3+} ions. The process of ET can be understood by the energy level diagram, shown in the Fig. 3.11 (b). As in the Fig. 3.11 (b), the $^3P_1$ level of Bi^{3+} ions is excited with 308 nm and the ET from the Bi^{3+} excited energy levels to Sm^{3+} levels takes place. The $^1S_0 \rightarrow {}^3P_1$ transition is allowed due to spin-orbit coupling and as a result Bi^{3+} ions are promoted to $^3P_1$ level. The $^3P_1$ level of Bi^{3+} ions lie close to the excited levels of Sm^{3+}, this prompts ET from Bi^{3+} ions to Sm^{3+} ions and we see an increase in emission peak intensity of Bi^{3+} co-doped phosphors when excited with 308 nm wavelength. The PL intensity observed upon 308 nm excitation is larger than the 404 nm excitation. However, the wLED application requires near UV excitation and 404 nm excitation wavelength is better suited for this application.

3.3.6 Decay curve analysis

The normalised PL decay curves of SMS4 and SMB2 phosphors in logarithmic scale for $^4G_{5/2} \rightarrow {}^6H_{9/2}$ transition (645 nm) upon 404 nm excitation are depicted in Fig. 3.12. We have examined the decay curves by fitting them with the biexponential equation 3.6 [139]:

$$I(t) = I_0 + A_1\, exp\left(-\frac{t}{\tau_1}\right) + A_2\, exp\left(-\frac{t}{\tau_2}\right) \tag{3.6}$$

Where I_0 is the background intensity at a long time after excitation and I is the intensity after t seconds; fast and slow decay times are denoted by τ_1 and τ_2, respectively; A_1 and A_2 are the fitting constants. To calculate the average lifetime we have used the following equation 3.7 [139],

$$\tau_{avg} = (A_1\tau_1^2 + A_2\tau_2^2)/(A_1\tau_1 + A_2\tau_2) \tag{3.7}$$

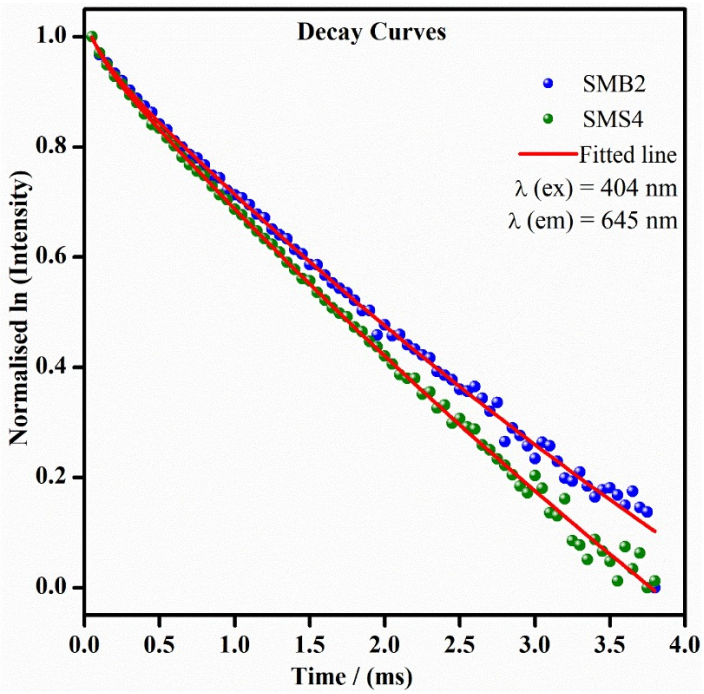

Fig. 3.12 Normalized logarithmic decay curves of **(a)** SMS4 and **(b)** SMB2 for $^4G_{5/2} \rightarrow {}^6H_{9/2}$ transition (645 nm) upon 404 nm excitation.

Using equations (3.1) and (3.2), the average lifetime of $^4G_{5/2}$ level of the Sm^{3+} ion for SMS4 and SMB2 is 9.8 ms and 11.4 ms, respectively. It was observed that the lifetime of Sm^{3+}

ions in $SrMoO_4:4Sm^{3+}$ increases by co-doping 2% Bi^{3+} ions because of the improved crystallinity. The improvement in crystallinity will decrease defect centers and total surface area, while increasing the number of emitting ions in the crystallites [138]. These all factors will reduce non-radiative relaxation and therefore the lifetime of Sm^{3+} ions increases [138–140]. Thus, from the decay curve analysis, the lifetime of $^4G_{5/2}$ level of the Sm^{3+} ions is found to increase in the presence of Bi^{3+} ions.

3.3.6 CIE study

The Commission Internationale de l'Elcairage (CIE) chromaticity diagram of SMS4, SMB1, SMB2, and SMB3 under 404 nm excitation and for spectra range from 500 to 750 nm is depicted in Fig. 3.13. The CIE coordinates calculated for SMS4 is 0.575, 0.419 and for SMB2 is 0.586, 0.410. The chromaticity diagram shows that slight shift in CIE coordinates towards red color by co-doping Bi^{3+} ions in the phosphors.

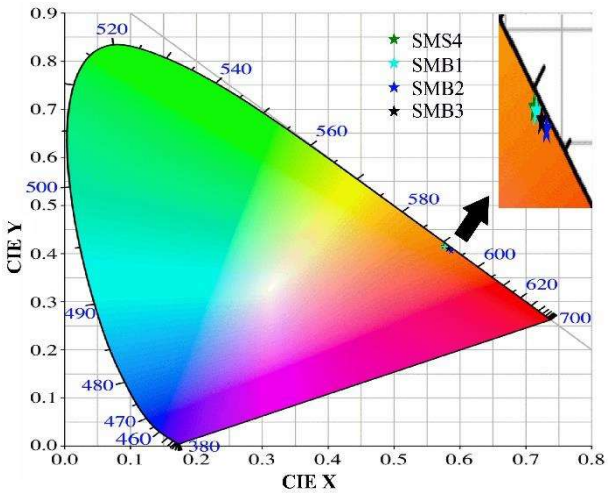

Fig. 3.13 CIE diagram for SMS4, SMB1, SMB2 and SMB3.

3.4 Conclusions

In summary, Sm^{3+} doped and Bi^{3+}/Sm^{3+} co-doped $SrMoO_4$ phosphors were successfully prepared by the cost-efficient solution combustion process. The XRD and FT-IR analysis authenticate the phase purity and vibrational modes of the prepared phosphors. The tailoring of the optical band gap of $SrMoO_4$ by doping Sm^{3+} and Bi^{3+} ions is studied by absorption spectroscopy. The Sm^{3+} doped phosphor emits reddish-orange emission centered at 645 nm due to $^4G_{5/2} \rightarrow {}^6H_{9/2}$ transition upon 404 nm excitation. This study reveals that the emission intensity of Sm^{3+} ion in $SrMoO_4$ phosphor can be further increased by co-doping Bi^{3+} ion. The co-doping of Bi^{3+} ions reduces the lattice strain and improves the crystallinity of the phosphor, thereby increasing the photoluminescence of $SrMoO_4$:$4Sm^{3+}$ when excited with 404 nm excitation wavelength. The decay curve analysis of the $^4G_{5/2}$ level of Sm^{3+} reveals that by co-doping Bi^{3+} ion, the crystal quality of the phosphors is improved which increases the lifetime of the $^4G_{5/2}$ level. Therefore, we ascertain that with suitable Bi^{3+} doping, Sm^{3+} co-doped $SrMoO_4$ phosphor may be a suitable candidate in the form of cost-efficient red phosphor for white light LEDs.